

Article

Transformation of H-Aggregates and J-Dimers of Water-Soluble Tetrakis (4-carboxyphenyl) Porphyrin in Polyion Complex Micelles

Shuai Liu ^{1,*}, Cun Hu ¹, Ying Wei ², Ming Duan ^{1,*}, Xin Chen ¹  and Yue Hu ¹

¹ College of Chemistry and Chemical Engineering, Southwest Petroleum University, Chengdu 610500, China; 201621000202@stu.swpu.edu.cn (C.H.); chenxin830107@pku.edu.cn (X.C.); 201721000233@stu.swpu.edu.cn (Y.H.)

² Beijing National Laboratory for Molecular Sciences, Institution College of Chemistry and Molecular Engineering, Peking University, Beijing 100871, China; 1601110376@pku.edu.cn

* Correspondence: 201599010093@swpu.edu.cn (S.L.); mduan@swpu.edu.cn (M.D.); Tel.: +86-028-8303-7346 (S.L. & M.D.)

Received: 4 April 2018; Accepted: 28 April 2018; Published: 3 May 2018



Abstract: Tetrakis (4-carboxyphenyl) porphyrin (TCPP) and polyelectrolyte poly(*N*-methyl-2-vinylpyridinium iodide)-*b*-poly(ethylene oxide) (PMVP₄₁-*b*-PEO₂₀₅) can self-aggregate into polyion complex (PIC) micelles in alkaline aqueous solution. UV-vis spectroscopy, fluorescence spectroscopy, transmission electron microscope, and dynamic light scattering were carried out to study PIC micelles. Density functional theory (DFT) calculation method was applied to study the interaction of TCPP and PMVP₄₁-*b*-PEO₂₀₅. We found that the H-aggregates and J-dimers of anionic TCPP transformed in PIC micelles. H-aggregates of TCPP formed at the charge ratio of TCPP/PMVP₄₁-*b*-PEO₂₀₅ 1:2 and J-dimer species at the charge ratio above 1:4, respectively. It is worth noting that the transformation from H-aggregates to J-dimer species of TCPP occurred just by adjusting the ratio of polymer and TCPP rather than by changing other factors such as pH, temperature, and ions.

Keywords: H-aggregates; J-dimers; transformation; porphyrin; PIC

1. Introduction

Water-soluble porphyrins have stimulated tremendous research attention owing to their potential applications in medical science, electronic equipment, biomimetic chemistry, and materials chemistry [1–4]. Since the relevant applications of water-soluble porphyrins are closely related with their aggregates, great efforts have been devoted to studying the aggregates of water-soluble porphyrins in recent years [5–9]. For example, Shi and co-workers have reported that the dimer and monomer of Fe^{III}-tetra(4-sulfonatophenyl)-porphyrin (Fe^{III}TPPS) aggregated to form complex micelles when they adjusted the pH value [10]. Tetrakis (4-carboxyphenyl) porphyrin is a well-researched dye due to its ability to self-aggregate into dimer species, J-aggregates (side-by-side arrangement), or H-aggregates (face-to-face arrangement) driven by non-covalently interactions. Some factors, such as a certain pH, changeable ionic strength, different solvents, temperature, and polymer template [11–17], have been reported to exert significant effects on the transformation of TCPP aggregates.

On the other hand, polyion complex (PIC) micelles have drawn increasing interest in the field of supermolecular self-assembly since they have great potential applications in controlled release [18], transduction of genes [19], delivery of biomolecules [20], nanoreactors [21], and sensors [22]. One of the characteristics of PIC micelles is that they often have core-shell structures, where the micellar core is deeply buried in the forest of the corona [23]. Thus, it is difficult for small molecules to diffuse into the core of micelles. On the contrary, the component that is incorporated in the micellar core is well

PMVP₄₁-*b*-PEO₂₀₅ aqueous solutions were fully mixed to obtain a solution with a charge ratio between TCPP and PMVP₄₁-*b*-PEO₂₀₅ is 1:0, 1:1, 1:2, 1:5 and 1:8. The charge ratio f is defined as follows: $f = \frac{[-]}{[+]}$, where $[-]$ refers to the concentration of negative charges carried by TCPP and $[+]$ refers to the concentration of positive charges carried by the PMVP₄₁ block. The final concentration of TCPP is 20 μ M, the pH of all above solutions at 10.0 ± 0.2 . When the concentration of TCPP is 5 μ M, the TCPP/PMVP₄₁-*b*-PEO₂₀₅ solutions were prepared in the same way. All experiments were carried out at room temperature unless otherwise specified.

A UV-1800 spectrophotometer (Shimadzu, Kyoto, Japan) operating in the range of 200~800 nm was used to measure the absorption of solution samples.

A LS55 Fluorescence Spectrometer (PerkinElmer, Waltham, MA, USA) was employed to measure the fluorescence (FL) emission of solution samples. According to the absorption, excitation, and emission spectra (shown in Figure S1), the excitation wavelength was set at 400 nm. Emission spectra were recorded in the range of 570~800 nm.

An ALV/DLS/SLS5022F light-scattering apparatus (Alv-Laser Vertriebsgesellschaft M-B.H., Langen, Germany) was applied to conduct dynamic light scattering (DLS) measurements. The apparatus was equipped with a 22 mW He–Ne laser (632.8 nm wavelength) with a refractive index matching bath of filtered toluene surrounding the cylindrical scattering cell. The samples were filtered through a 450 nm membrane filter. The scattering angle was set at 90° .

A JEOL-100CX II transmission electron microscope (TEM, JEOL, Tokyo, Japan) was used to observe the morphology of the self-assembled micelles. Typically, a drop of sample was placed onto 230 mesh copper grids coated with Formvar film and negatively stained. Then, the sample was allowed to dry naturally for TEM observation.

A steady-state spectrometer FLS920 was applied to determine the decay times of the TCPP/PMVP₄₁-*b*-PEO₂₀₅ systems, the excitation wavelength was 400 nm. The fluorescence decays were analyzed using DAS6 software. The experimental time-resolved fluorescence decays can be analyzed using a reported formula [30]:

$$R(t) = b + \sum_i^n \alpha_i \exp\left(-\frac{t}{\tau_i}\right),$$

where b is the baseline correction, n is the number of discrete emissive species, and α_i and τ_i are the pre-exponential factors and excited-state fluorescence lifetimes associated with the i th component, respectively.

The calculations were performed within the spin-unrestricted density functional theory (DFT) framework implemented in the DMol3 code [31–33]. The generalized gradient approximation (GGA) with the BLYP functional [34,35], together with double numeric quality basis set (DNP), was used in all calculations. The convergence tolerance for energy change, max displacement, and max force were 2×10^{-5} Ha, 0.005 Å, and 0.004 Ha Å⁻¹, respectively.

3. Results and Discussion

3.1. Aggregation Behavior of TCPP at Various Concentrations

UV-vis spectroscopy was used to measure the critical aggregation concentration of TCPP. Figure 1a shows that the absorption intensity increases as the concentration of TCPP increases. The maximum absorption peak of TCPP is 414.5 nm when the concentration is less than 6 μ M. At the range of 1.0~5.0 μ M, the intensity of maximum absorption peak increased in a linear fashion, as shown in Figure 1b, which fits the Lambert–Beer Law. In an alkaline aqueous solution and low concentration, TCPP molecules exist in the form of a monomeric free base (TCPP⁴⁻) due to electrostatic repulsion between TCPP⁴⁻. Meanwhile, the deviations from Beer's law at high concentrations (above 5.0 μ M) have been well documented and this phenomenon is usually ascribed to the formation of aggregates [36–38]. The strongest absorption peak shifted from 414.5 nm to 416.5 nm (Table S1) and

split into two peaks when the concentration of TCPP is above 6.0 μM (detailed spectra shown in Figure S2). The slight blue shift of max absorption and its split are considered to be due to the formation of J-dimers rather than J-aggregates under these conditions [39] since the concentration of TCPP > 5 μM is consistent with that previously reported to yield dimerization behavior [40].

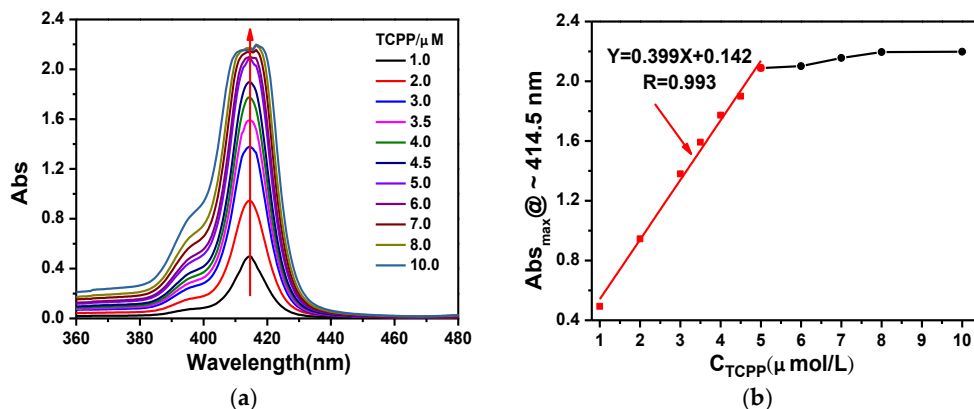


Figure 1. (a) UV-vis absorption spectra and (b) maximum absorption at ~ 414.5 nm of TCPP solutions at various concentrations. Red line fits the Lambert–Beer Law, $R = 0.993$. Black line deviates from Beer’s law.

3.2. PIC Micelles Formed by TCPP and PMVP_{41-b}-PEO₂₀₅

At a concentration of 20 μM , TCPP molecules mainly exist in the form of J-dimers in alkaline aqueous solution. Upon mixing with the positively charged double hydrophilic block copolymer PMVP_{41-b}-PEO₂₀₅, a strong Tyndall effect was observed, suggesting the formation of polyion complex micelles (PIC). TEM observations (Figure 2) confirmed the formation of PIC. As can be seen, the average diameter of the micelles are about 20–30 nm, 90–100 nm, 100–130 nm, and 200 nm at charge ratios of TCPP and PMVP_{41-b}-PEO₂₀₅ of 1:1, 1:2, 1:5, and 1:8, respectively, which are larger than those of micelles (9 nm, Figure 3f) formed with PMVP_{41-b}-PEO₂₀₅.

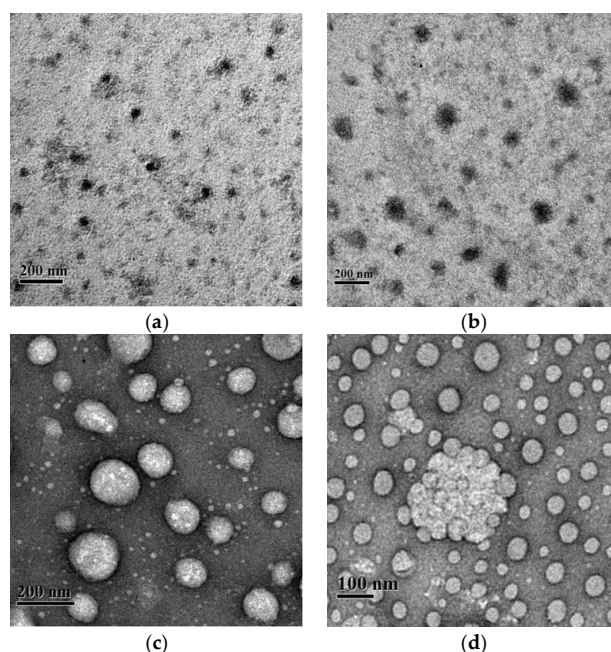


Figure 2. TEM images of polyion complex micelles formed by TCPP and PMVP_{41-b}-PEO₂₀₅ at the charge ratios of (a) 1:1; (b) 1:2; (c) 1:5 and (d) 1:8.

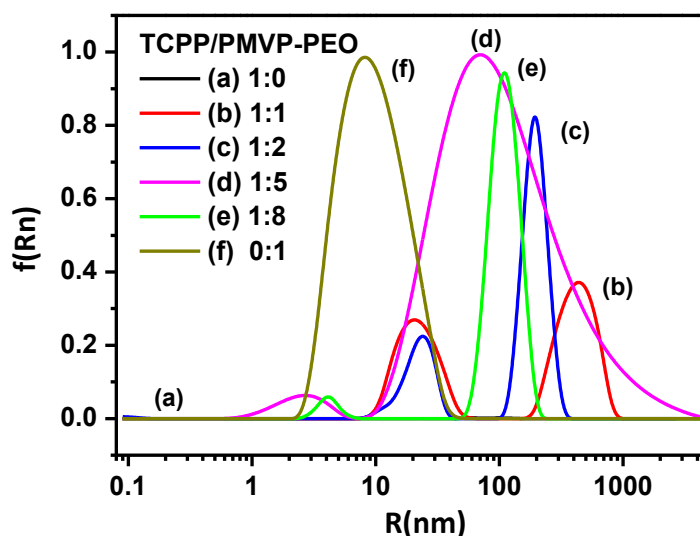


Figure 3. DLS results of polyion complex micelles formed by TCPP and PMVP₄₁-*b*-PEO₂₀₅ at the charge ratios of (a) 1:0; (b) 1:1; (c) 1:2; (d) 1:5; (e) 1:8 and (f) 0:1. PMVP-PEO is an abbreviation of PMVP₄₁-*b*-PEO₂₀₅.

In addition, the overall hydrodynamic radius of the micelles was also measured with dynamic light scattering (DLS) as shown in Figure 3. In the absence of polymers, no micelles of TCPP were found, which also proves that TCPP exists in the form of J-dimers instead of J-aggregates. The aggregates of PMVP₄₁-*b*-PEO₂₀₅ (20 nm) and TCPP/PMVP₄₁-*b*-PEO₂₀₅ (500 nm, not observed under TEM) exist at the same time at the charge ratio is 1:1. As the charge ratio is increased to 1:2, the TCPP and PMVP₄₁-*b*-PEO₂₀₅ co-assemble into large aggregates and coexist with the small micelles in the solution. At 1:5, the average hydrodynamic radius of the particles and their polydispersity were observed to strongly increase, which is ascribed to the aggregation of the micelles into large micelles or clusters (Figure 2c,d). For a 1:8 system, the clusters are dominant, which can be observed under TEM, and the dispersion is narrowed.

3.3. H-Aggregates and J-Dimers' Transformation of TCPP in PIC Micelles

The formation of PIC micelles leads to a significant change in the UV-vis absorption of TCPP. Figure 4 displays the UV-vis spectrum of TCPP in aqueous solution when it is mixed with the polymer PMVP₄₁-*b*-PEO₂₀₅. The black line reveals the characteristic features of TCPP, an intense Soret band at 416.5 nm and four weak Q bands at 517.0, 554.5, 580.5 and 635.0 nm. Upon the formation of micelles, the Soret band of TCPP was blue shifted from 416.5 nm to 406.5 as the charge ratio of TCPP and PMVP₄₁-*b*-PEO₂₀₅ at 1:2 and the intensity did not change significantly. The blue shift of sharp and narrow absorption bands indicate the formation of H-aggregates [41]. Moreover, the Q bands appear to exhibit an etio pattern [40] along with decreasing intensities and increasing wavelengths. The red shift of TCPP on the Q band is attributed to the process of TCPP interacting with other components. The red shift of the Q band is caused by the reduction of the energy gap between the highest occupied molecular orbital and the lowest unoccupied molecular orbital [42]. These results suggest that the interaction between TCPP and the polymer in PIC micelles has changed the local environment of TCPP [43].

However, as the concentration of PMVP₄₁-*b*-PEO₂₀₅ increased further, the strongest peak moved back to 416.5 nm (Table S2). From this phenomenon, it can be inferred that H-aggregates disappeared and the TCPP molecules exist in the form of J-dimers again. These results are similar to the behaviors in acidic TCPP solutions [44]. The TCPP molecules in the core of PIC micelles exist in the form of H-aggregates at a ratio < 1:4, but still exist in the form of J-dimers at a ratio > 1:4. Moreover, the formation of J-dimers is considered to be due to the formation of PIC micelles rather than ionic

strengths, since these experiments are performed at ionic strengths (<50 mM) well below those that correlate with dimerization [45]. In addition, the absorption of TCPP at a concentration of 5 μM was also tested. The absorption spectra are similar to the above results. Detailed data are shown in Figure S3.

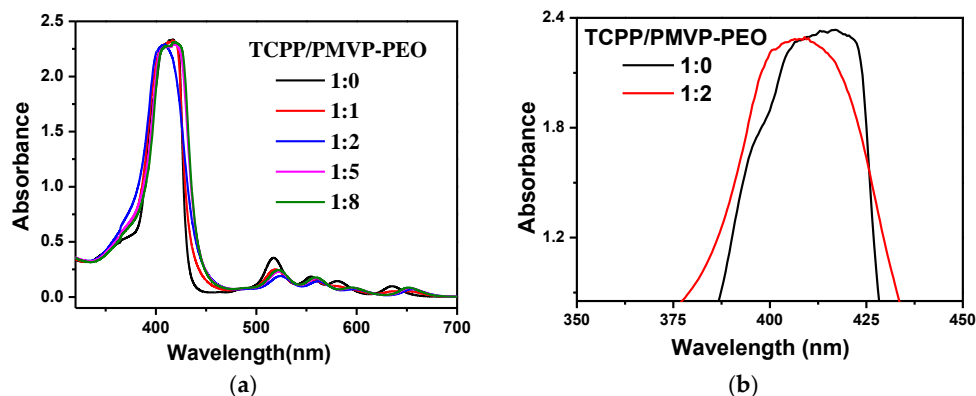


Figure 4. (a) UV-vis absorption spectra of TCPP (black line) and TCPP/PMVP-PEO with different charge ratios of 1:0 (black line), 1:1 (red line), 1:2 (blue line), 1:5 (pink line) and 1:8 (green line), respectively; (b) Magnified absorption spectra of TCPP and TCPP/PMVP-PEO at the charge ratio of 1:2. [TCPP] = 0.02 mM, pH = 10.0. PMVP-PEO is the abbreviation of PMVP₄₁-*b*-PEO₂₀₅.

The fluorescence spectra of the TCPP and PMVP₄₁-*b*-PEO₂₀₅ aggregates at different charge ratios in alkaline aqueous solution are shown in Figure 5. As can be seen, TCPP shows two intense emission bands at 645 nm and 702 nm. With the addition of PMVP₄₁-*b*-PEO₂₀₅, fluorescence intensity decreases when the charge ratios are 1:1 and 1:2. At the charge ratio 1:2, the fluorescence intensity is the lowest and the peak position is red-shifted, which is ascribed to the formation of H-aggregates among TCPP. As the charge ratio is greater than 1:2, the fluorescence intensity increases and the peak position exhibits a blue shift. This phenomenon is ascribed to the transformation from H-aggregates to J-dimers of TCPP [46]. The fluorescence spectra are similar to the above results when the concentration of TCPP is 5 μM . Detailed data are shown in Figure S4.

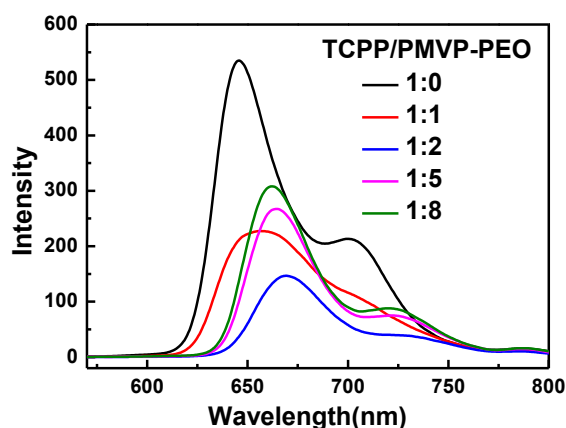


Figure 5. Fluorescence spectra of TCPP (black line) and TCPP/PMVP-PEO with different charge ratios of 1:1 (red line), 1:2 (blue line), 1:5 (pink line) and 1:8 (green line). [TCPP] = 0.02 mM, pH = 10.0, λ_{ex} = 400 nm. PMVP-PEO is an abbreviation of PMVP₄₁-*b*-PEO₂₀₅.

To understand the aggregates transformation of TCPP in the PIC micelles, we carried out fluorescence lifetime measurements. The fluorescence decay curves of the TCPP/PMVP₄₁-*b*-PEO₂₀₅ systems in alkaline aqueous solution are shown in Figure 6. As can be seen, the TCPP afforded a

monoexponential fluorescence decay curve with a characteristic lifetime around 9.65 ns. Meanwhile, the other decay curves are fitted biexponentially. At a charge ratio of 1:2, the decay components are 8.2 ns and 10.3 ns and the average decay time is 9.25 ns. The shortening of decay time of TCPP aggregates from TCPP-dimer unambiguously confirms the H-type aggregation of the TCPP molecules [47]. As the charge ratio reaches 1:5, the decay components are 9.25 ns and 10.2 ns and the average decay time is 9.72 ns. The decay time gradually returned to the dimer state as the concentration of the PMVP₄₁-*b*-PEO₂₀₅ increased, which unambiguously confirms the transformation of H-aggregates and J-dimers.

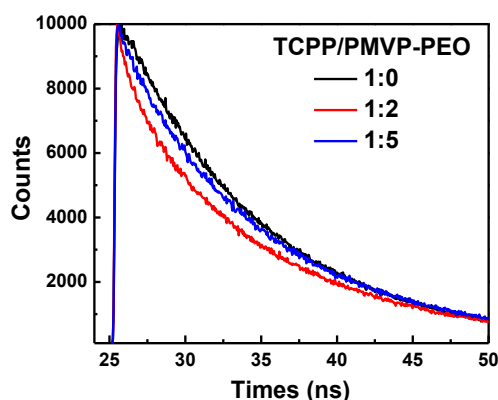


Figure 6. Fluorescence decay time of TCPP and TCPP/PMVP-PEO at different charge ratios of 1:0, 1:2, and 1:5. PMVP-PEO is an abbreviation of PMVP₄₁-*b*-PEO₂₀₅.

In order to investigate the influence of PIC micelle formation on the local environment of TCPP, the spin-unrestricted DFT method was employed to understand the effect of PIC on the energy distribution of TCPP. The structure of PMVP₄₁-*b*-PEO₂₀₅ was simplified and only one of the monomer units was applied in the calculation, labeled (PMVP-PEO)₁. Figure 7 shows the HOMO and LUMO of the TCPP before and after interacting with one unit of PMVP₄₁-*b*-PEO₂₀₅. As revealed, the energy gap between the HOMO and LUMO of TCPP is 1.76 eV, and it is reduced to 0.85 eV when it interacts with one unit of PMVP₄₁-*b*-PEO₂₀₅. This result is supported by the comparison of absorption spectra of TCPP before and after introduction of PMVP₄₁-*b*-PEO₂₀₅ (Figure 4). The addition of PMVP₄₁-*b*-PEO₂₀₅ induces red shift of the Q band of TCPP.

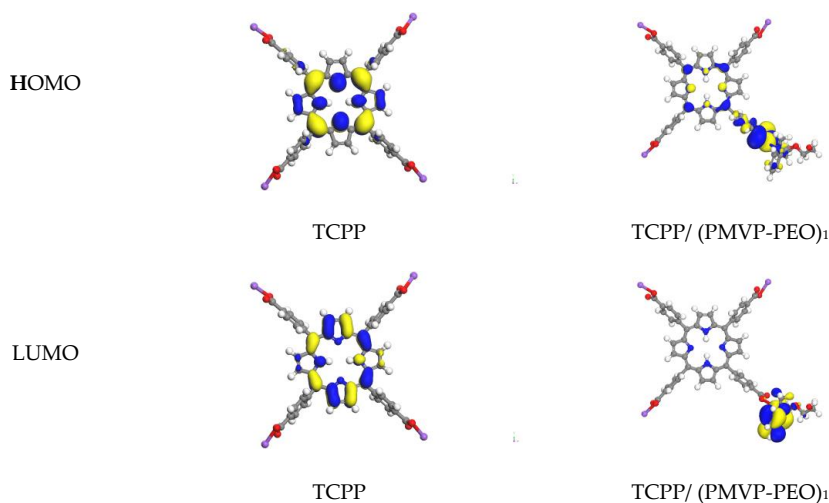
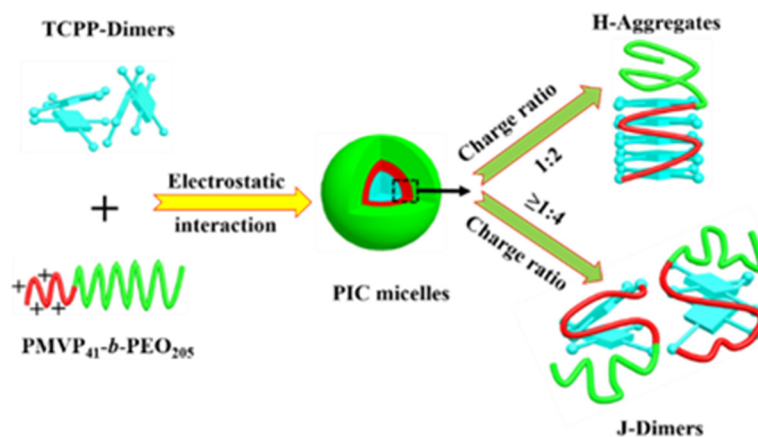


Figure 7. Molecular orbital diagrams calculated for TCPP and TCPP/ (PMVP-PEO)₁. PMVP-PEO is an abbreviation of PMVP₄₁-*b*-PEO₂₀₅.

With the integration of information indicated by TEM, DLS, UV-vis, FL and DFT analyses, it can be speculated that TCPP and PMVP_{41-b}-PEO₂₀₅ can self-aggregate into PIC micelles, which might be the reason for the H-aggregates and J-dimers' transformation of TCPP. The complete scenario for the aggregate transformation of TCPP is graphically depicted in Scheme 2 to facilitate comprehension of this process.



Scheme 2. Illustration of the self-assembly of the TCPP/PMVP_{41-b}-PEO₂₀₅ complex micelles and the transformation of H-aggregates and J-dimers of TCPP in PIC micelles.

4. Conclusions

The transformation from J-dimers to H-aggregates and further to J-dimers represents an interesting model to investigate the assembly, structure, and applications of a wide variety of fluorescent molecules aggregated in PIC micelles. In exploratory experiments, we have shown that a change of various forms can be achieved by adjusting the charge ratio of TCPP and PMVP_{41-b}-PEO₂₀₅. This result is of particular interest due to there being different advantages of different aggregates ranging from light harvesting capability to catalytic activity. Moreover, the versatility of various aggregates' formation through controlling the charge ratios of polymer and porphyrins may build a valuable basis for the use of PIC micelles in medicine and catalysis.

Supplementary Materials: The following are available online at <http://www.mdpi.com/2073-4360/10/5/494/s1>, Figure S1: Absorption and Fluorescence spectra of TCPP at different excitation. Figure S2: (a) The absorption spectra of TCPP at different concentrations and (b) Magnified absorption peak. Figure S3: UV-vis absorption spectra of TCPP and TCPP/PMVP_{41-b}-PEO₂₀₅ with different charge ratios. [TCPP] = 5 μM, pH = 10.0. Figure S4: Fluorescence spectra of TCPP and TCPP/PMVP_{41-b}-PEO₂₀₅ with different charge ratios. [TCPP] = 5 μM, pH = 10.0. Table S1: Maximum absorption peak at various concentrations of TCPP. Table S2: Character absorption peaks of TCPP at different charge ratios of TCPP and PMVP_{41-b}-PEO₂₀₅.

Author Contributions: Shuai Liu and Ming Duan conceived and designed the experiments; Cun Hu, Xin Chen, Yue Hu, and Ying Wei performed the experiments; Shuai Liu, Cun Hu and Ying Wei analyzed the data; Shuai Liu and Ming Duan contributed reagents/materials/analysis tools; Shuai Liu and Cun Hu wrote the paper.

Acknowledgments: This work was supported by the Young Scholars Development Fund of SWPU (201599010093), the National Natural Science Foundation of China (21703177), a Scientific Research Starting Project of SWPU (2017QHZ016), and the Sichuan Youth Science & Technology Foundation for Innovation Team (2015TD0007). We acknowledge the National Supercomputing Center in Shenzhen for providing the computational resources and materials studio (version 7.0, DMol3 module).

Conflicts of Interest: The authors declare no conflict of interest.

References

1. Kubat, P.; Lang, K.; Janda, P.; Anzenbacher, P., Jr. Interaction of porphyrins with a dendrimer template: Self-aggregation controlled by pH. *Langmuir* **2005**, *21*, 9714–9720. [CrossRef] [PubMed]

2. Lammi, R.K.; Ambrose, A.; Balasubramanian, T.; Wagner, R.W.; Bocian, D.F.; Holten, D.; Lindsey, J.S. Structural control of photoinduced energy transfer between adjacent and distant sites in multiporphyrin arrays. *J. Am. Chem. Soc.* **2000**, *122*, 7579–7591. [[CrossRef](#)]
3. Zhao, Q.; Wang, Y.; Qiao, Y.; Wang, X.; Guo, X.; Yan, Y.; Huang, J. Conductive porphyrin helix from ternary self-assembly systems. *Chem. Commun.* **2014**, *50*, 13537–13539. [[CrossRef](#)] [[PubMed](#)]
4. Yamanishi, K.; Yairi, T.; Suzuki, K.; Kondo, M. Biomimic O-2 activation hydroxylates a meso-carbon of the porphyrin ring regioselectively under mild conditions. *Chem. Commun.* **2013**, *49*, 9296–9298. [[CrossRef](#)] [[PubMed](#)]
5. Zhao, L.; Wang, X.; Li, Y.; Ma, R.; An, Y.; Shi, L. Chiral micelles of achiral TPPS and diblock copolymer induced by amino acids. *Macromolecules* **2009**, *42*, 6253–6260. [[CrossRef](#)]
6. Zhao, L.; Ma, R.; Li, J.; Li, Y.; An, Y.; Shi, L. J- and H-aggregates of 5,10,15,20-tetrakis-(4-sulfonatophenyl)-porphyrin and interconversion in PEG-b-P4VP micelles. *Biomacromolecules* **2008**, *9*, 2601–2608. [[CrossRef](#)] [[PubMed](#)]
7. Li, A.; Zhao, L.; Hao, J.; Ma, R.; An, Y.; Shi, L. Aggregation behavior of the template-removed 5,10,15,20-tetrakis(4-sulfonatophenyl)porphyrin chiral array directed by poly(ethylene glycol)-block-poly(L-lysine). *Langmuir* **2014**, *30*, 4797–4805. [[CrossRef](#)] [[PubMed](#)]
8. Zhao, L.; Xiang, R.; Ma, R.; Wang, X.; An, Y.; Shi, L. Chiral conversion and memory of TPPS J-aggregates in complex micelles: PEG-b-PDMAEMA/TPPS. *Langmuir* **2011**, *27*, 11554–11559. [[CrossRef](#)] [[PubMed](#)]
9. Yamamoto, S.; Nagatani, H.; Imura, H. Potential-induced aggregation of anionic porphyrins at liquid | liquid interfaces. *Langmuir* **2017**. [[CrossRef](#)] [[PubMed](#)]
10. Zhao, L.; Li, A.; Xiang, R.; Shen, L.; Shi, L. Interaction of FEIII-Tetra-(4-sulfonatophenyl)-porphyrin with copolymers and aggregation in complex micelles. *Langmuir* **2013**, *29*, 8936–8943. [[CrossRef](#)] [[PubMed](#)]
11. Liu, Q.; Zhou, H.; Zhu, J.; Yang, Y.; Liu, X.; Wang, D.; Zhang, X.; Zhuo, L. Self-assembly into temperature dependent micro-/nano-aggregates of 5,10,15,20-tetrakis(4-carboxyl phenyl)-porphyrin. *Mater. Sci. Eng. C-Mater.* **2013**, *33*, 4944–4951. [[CrossRef](#)] [[PubMed](#)]
12. Mandal, S.; Nayak, S.K.; Mallampalli, S.; Patra, A. Surfactant-assisted porphyrin based hierarchical nano/micro assemblies and their efficient photocatalytic behavior. *ACS Appl. Mater. Interfaces* **2014**, *6*, 130–136. [[CrossRef](#)] [[PubMed](#)]
13. Ohno, O.; Kaizu, Y.; Kobayashi, H. J-aggregate formation of a water-soluble porphyrin in acidic aqueous media. *J. Chem. Phys.* **1993**, *99*, 4128–4139. [[CrossRef](#)]
14. Maiti, N.C.; Shyamalava Mazumdar, A.; Periasamy, N. J- and H-aggregates of porphyrin–surfactant complexes: Time-resolved fluorescence and other spectroscopic studies[†]. *J. Phys. Chem. B* **1998**, *102*, 1528–1538. [[CrossRef](#)]
15. Akins, D.L.; Zhu, H.R.; Guo, C. Absorption and raman scattering by aggregated meso-tetrakis(p-sulfonatophenyl) porphine. *J. Phys. Chem.* **1994**, *98*, 3612–3618. [[CrossRef](#)]
16. Jiang, S.; Zhang, L.; Liu, M. Photo-triggered J-aggregation and chiral symmetry breaking of an anionic porphyrin (TPPS) in mixed organic solvent. *Chem. Commun.* **2009**, *41*, 6252–6254. [[CrossRef](#)] [[PubMed](#)]
17. Sugikawa, K.; Takamatsu, Y.; Yasuhara, K.; Ueda, M.; Ikeda, A. Reversible vesicle-to-disk transitions of liposomes induced by the self-assembly of water-soluble porphyrins. *Langmuir* **2017**, *33*, 1023–1029. [[CrossRef](#)] [[PubMed](#)]
18. Zhang, Q.; Ko, N.R.; Oh, J.K. Recent advances in stimuli-responsive degradable block copolymer micelles: Synthesis and controlled drug delivery applications. *Chem. Commun.* **2012**, *48*, 7542–7552. [[CrossRef](#)] [[PubMed](#)]
19. Oe, Y.; Christie, R.J.; Naito, M.; Low, S.A.; Fukushima, S.; Toh, K.; Miura, Y.; Matsumoto, Y.; Nishiyama, N.; Miyata, K.; et al. Actively-targeted polyion complex micelles stabilized by cholesterol and disulfide cross-linking for systemic delivery of sirna to solid tumors. *Biomaterials* **2014**, *35*, 7887–7895. [[CrossRef](#)] [[PubMed](#)]
20. Yang, X.-Z.; Du, X.-J.; Liu, Y.; Zhu, Y.-H.; Liu, Y.-Z.; Li, Y.-P.; Wang, J. Rational design of polyion complex nanoparticles to overcome cisplatin resistance in cancer therapy. *Adv. Mater.* **2014**, *26*, 931–936. [[CrossRef](#)] [[PubMed](#)]
21. Palivan, C.G.; Fischer-Onaca, O.; Delcea, M.; Ite, F.; Meier, W. Protein-polymer nanoreactors for medical applications. *Chem. Soc. Rev.* **2012**, *41*, 2800–2823. [[CrossRef](#)] [[PubMed](#)]

22. Cabral, H.; Miyata, K.; Kishimura, A. Nanodevices for studying nano-pathophysiology. *Adv. Drug Deliv. Rev.* **2014**, *74*, 35–52. [[CrossRef](#)] [[PubMed](#)]
23. Wang, J.; Velders, A.H.; Gianolio, E.; Aime, S.; Vergeldt, F.J.; Van As, H.; Yan, Y.; Drechsler, M.; de Keizer, A.; Stuart, M.A.C.; et al. Controlled mixing of lanthanide(III) ions in coacervate core micelles. *Chem. Commun.* **2013**, *49*, 3736–3738. [[CrossRef](#)] [[PubMed](#)]
24. Takemoto, H.; Ishii, A.; Miyata, K.; Nakanishi, M.; Oba, M.; Ishii, T.; Yamasaki, Y.; Nishiyama, N.; Kataoka, K. Polyion complex stability and gene silencing efficiency with a sirna-grafted polymer delivery system. *Biomaterials* **2010**, *31*, 8097–8105. [[CrossRef](#)] [[PubMed](#)]
25. Purrello, R.; Bellacchio, E.; Gurrieri, S.; Lauceri, R.; Raudino, A.; Scolaro, L.M.; Santoro, A.M. pH modulation of porphyrins self-assembly onto polylysine. *J. Phys. Chem. B* **1998**, *102*, 8852–8857. [[CrossRef](#)]
26. Ruthard, C.; Maskos, M.; Kolb, U.; Grohn, F. Polystyrene sulfonate–porphyrin assemblies: Influence of polyelectrolyte and porphyrin structure. *J. Phys. Chem. B* **2011**, *115*, 5716–5729. [[CrossRef](#)] [[PubMed](#)]
27. And, A.H.; Kataoka, K. Novel polyion complex micelles entrapping enzyme molecules in the core: Preparation of narrowly-distributed micelles from lysozyme and poly(ethylene glycol)–poly(aspartic acid) block copolymer in aqueous medium. *Macromolecules* **1998**, *31*, 288–294.
28. Biesalski, M.; Johannsmann, D. Electrolyte-induced collapse of a polyelectrolyte brush. *J. Chem. Phys.* **2004**, *120*, 8807–8814. [[CrossRef](#)] [[PubMed](#)]
29. Wu, Z.; Huang, J.; Yan, Y. Electrostatic polyion micelles with fluorescence and MRI dual functions. *Langmuir* **2015**, *31*, 7926–7933. [[CrossRef](#)] [[PubMed](#)]
30. Mandal, S.; Rahaman, M.; Sadhu, S.; Nayak, S.K.; Patra, A. Fluorescence switching of quantum dot in quantum dot–porphyrin–cucurbit [7] uril assemblies. *J. Phys. Chem. C* **2013**, *117*, 3069–3077. [[CrossRef](#)]
31. Delley, B. An all-electron numerical method for solving the local density functional for polyatomic molecules. *J. Chem. Phys.* **1990**, *92*, 508–517. [[CrossRef](#)]
32. Delley, B. Fast calculation of electrostatics in crystals and large molecules. *J. Phys. Chem.* **1996**, *100*, 6107–6110. [[CrossRef](#)]
33. Delley, B. From molecules to solids with the DMol3 approach. *J. Chem. Phys.* **2000**, *113*, 7756–7764. [[CrossRef](#)]
34. Becke, A.D. A multicenter numerical integration scheme for polyatomic molecules. *J. Chem. Phys.* **1988**, *88*, 2547–2553. [[CrossRef](#)]
35. Lee, C.; Yang, W.; Parr, R.G. Development of the colle-salvetti correlation energy formula into a functional of the electron density. *Phys. Rev. B* **1988**, *37*, 785–789. [[CrossRef](#)]
36. Kang, Y.T.; Cai, Z.G.; Tang, X.Y.; Liu, K.; Wang, G.T.; Zhang, X. An amylase-responsive bolaform supra-amphiphile. *ACS Appl. Mater. Interfaces* **2016**, *8*, 4927–4933. [[CrossRef](#)] [[PubMed](#)]
37. Liu, B.W.; Guo, D.S.; Song, B.A. Aggregation behaviors of novel dicationic porphyrin and ultrasound-induced aggregation transformation. *Sci. Sin. Chim.* **2011**, *41*, 741–747. [[CrossRef](#)]
38. Helmich, F.; Lee, C.C.; Nieuwenhuizen, M.M.; Gielen, J.C.; Christianen, P.C.; Larsen, A.; Fytas, G.; Leclère, P.E.; Schenning, A.P.; Meijer, E.W. Dilution-induced self-assembly of porphyrin aggregates: A consequence of coupled equilibria. *Angew. Chem.* **2010**, *49*, 3939–3942. [[CrossRef](#)] [[PubMed](#)]
39. Choi, M.Y.; Pollard, J.A.; Webb, M.A.; McHale, J.L. Counterion-dependent excitonic spectra of tetra(p-carboxyphenyl)porphyrin aggregates in acidic aqueous solution. *J. Am. Chem. Soc.* **2003**, *125*, 810–820. [[CrossRef](#)] [[PubMed](#)]
40. Clarke, S.E.; Wamser, C.C.; Bell, H.E. Aqueous complexation equilibria of meso-tetrakis(4-carboxyphenyl) porphyrin with viologens: Evidence for 1:1 and 1:2 complexes and induced porphyrin dimerization. *J. Phys. Chem. A* **2002**, *106*, 3235–3242. [[CrossRef](#)]
41. Zhang, X.F.; Xi, Q.; Zhao, J. Fluorescent and triplet state photoactive j-type phthalocyanine nano assemblies: Controlled formation and photosensitizing properties. *J. Mater. Chem.* **2010**, *20*, 6726–6733. [[CrossRef](#)]
42. Gandini, S.C.M.; Yushmanov, V.E.; And, I.E.B.; Tabak, M. Interaction of the tetra(4-sulfonatophenyl)porphyrin with ionic surfactants: Aggregation and location in micelles. *Langmuir* **1999**, *15*, 6233–6243. [[CrossRef](#)]
43. Zheng, R.; Wu, Z.; Yan, Y.; Wang, J.; Huang, J. Suppressing singlet oxygen formation from 5,10,15,20-tetrakis(4-sulfonatophenyl)porphyrin using polyion complex micelles. *RSC Adv.* **2015**, *5*, 17253–17256. [[CrossRef](#)]
44. Zhao, L.; Xiang, R.; Zhang, L.; Wu, C.; Ma, R.; An, Y.; Shi, L. Micellization of copolymers via noncovalent interaction with TPPS and aggregation of TPPS. *Sci. China Chem.* **2011**, *54*, 343–350. [[CrossRef](#)]

45. Pasternack, R.F.; Huber, P.R.; Boyd, P.; Engasser, G.; Francesconi, L.; Gibbs, E.; Fasella, P.; Venturo, G.C.; Hinds, L.D.C. On the aggregation of meso-substituted water-soluble porphyrins. *J. Am. Chem. Soc.* **1972**, *94*, 4511–4517. [[CrossRef](#)] [[PubMed](#)]
46. Doan, S.C.; Shanmugham, S.; Aston, D.E.; McHale, J.L. Counterion dependent dye aggregates: Nanorods and nanorings of tetra(p-carboxyphenyl)porphyrin. *J. Am. Chem. Soc.* **2005**, *127*, 5885–5892. [[CrossRef](#)] [[PubMed](#)]
47. Tozoni, J.R.; Neto, N.M.B.; Ribeiro, C.A.; Pazin, W.M.; Ito, A.S.; Borissevitch, I.E.; Marletta, A. Relationship between porphyrin aggregation and formation of porphyrin ring structures in poly(*N*-alkyl methacrylate)/porphyrin blends. *Polymer* **2016**, *102*, 136–142. [[CrossRef](#)]



© 2018 by the authors. Licensee MDPI, Basel, Switzerland. This article is an open access article distributed under the terms and conditions of the Creative Commons Attribution (CC BY) license (<http://creativecommons.org/licenses/by/4.0/>).